

Generation of ultrarelativistic vortex leptons with large orbital angular momenta

Mamutjan Ababekri,¹ Jun-Lin Zhou,¹ Ren-Tong Guo,¹ Yong-Zheng Ren,¹ Yu-Han Kou,¹ Qian Zhao,¹ Zhong-Peng Li,¹ and Jian-Xing Li^{1,2,*}

¹*Ministry of Education Key Laboratory for Nonequilibrium Synthesis and Modulation of Condensed Matter, Shaanxi Province Key Laboratory of Quantum Information and Quantum Optoelectronic Devices, School of Physics, Xi'an Jiaotong University, Xi'an 710049, China*

²*Department of Nuclear Physics, China Institute of Atomic Energy, P. O. Box 275(7), Beijing 102413, China*

(Dated: October 25, 2024)

We put forward a novel method for generating ultrarelativistic vortex positrons and electrons with intrinsic orbital angular momenta (OAM) through nonlinear Breit-Wheeler (NBW) scattering of vortex γ photons. A complete angular momentum-resolved scattering theory has been formulated, introducing angular momenta of laser photons and vortex particles into the conventional NBW scattering framework. We find that vortex positron (electron) can be produced when the outgoing electron (positron) is generated along the collision axis. By unveiling the angular momentum transfer mechanism, we clarify that the OAM of the γ photon and the large angular momenta due to multiple laser photons are entirely transferred to the generated vortex leptons. Furthermore, the cone opening angle and superposition state of the vortex γ photon can be determined via the angular distribution of created pairs in NBW processes.

I. INTRODUCTION

Vortex particles with intrinsic orbital angular momenta (OAM) exhibit wave packets featuring helical phase fronts [1–4]. They can introduce novelty to scattering processes owing to their distinctive properties, including large angular momenta (AM) and helical wave fronts [5–8]. Collision of ultrarelativistic vortex particle beams presents an opportunity to expand the scope of future colliders [9–11]. Utilizing ultrarelativistic vortex leptons in deep inelastic scattering experiments has the potential to provide new insight into the spin and OAM constituents of protons, offering potential solutions to the long-standing proton spin puzzle [12–15]. Currently, vortex electrons can be produced with kinetic energy up to about 300 keV using spiral phase plates, fork diffraction gratings, or magnetic needles [16–18]. Neutrons and atoms can also be brought into vortex states using similar wave front engineering techniques at low energies [19–23]. Unfortunately, the generation of ultrarelativistic ones remains a great challenge.

In theory, charged particles can be initially prepared in vortex states at low energies and then accelerated to high energies [24–26]. Their precise behavior during high-energy acceleration and the preservation of vortex structures in practical external fields require theoretical investigation and await experimental verification [7]. Another approach to producing high-energy vortex particles involves collision events, utilizing the entanglement of final state particles in scattering processes [27–32]. In this scenario, one final particle can acquire a vortex state if specific postselection procedures are applied to the other. For instance, a generalized measurement can be employed and measures the azimuth angle of the final particle with significant uncertainty to induce the vortex state in the other particle [31]. However, generalized measurement is known only for low-energy processes [33, 34], and implementing it in high-energy collisions poses substantial

challenges. Another possibility is demonstrated for the Compton scattering process, in which the helical wave front is transferred from the initial vortex photon to the final vortex γ photon if the final electron is scattered along the collision axis [27]. Lepton-antilepton pairs can be created through the conversion of light into matter, as demonstrated in the Breit-Wheeler (BW) or Bethe-Heitler (BH) scattering processes [35–42]. There are proposals for generating vortex pairs via linear BW and BH processes by assuming a twisted detector that performs coherent vortex postselection over final particles [43–45]. However, the possibility of generating vortex leptons through a feasible postselection scenario with a considerable probability in pair creation dynamics remains unknown.

Meanwhile, using ultrashort and ultraintense laser pulses [46–50], the nonlinear Breit-Wheeler (NBW) scattering has emerged as a promising method for generating high-brilliance and high-energy positron beams [51–54]. Recent advancements in this field have also revealed the related polarization features, allowing for the production of polarized pairs [55–63]. However, it is worth noting that current studies focus on investigating the spin angular momentum (SAM) as the only internal degree of freedom [64–71]. Furthermore, since NBW pair creation entails the absorption of multiple laser photons, a substantial amount of AM carried by photons in the laser field is expected to be transferred to the generated pairs. While the overall beam in NBW processes may acquire extrinsic (mechanical) OAM [72–75], the intrinsic OAM carried by scattering particles (γ photons, electrons, and positrons) remain unknown. Consequently, the AM transfer mechanism and the formation of a helical wave front in the final state during NBW processes are still unclear, leaving the generation of ultrarelativistic vortex leptons in intense lasers an open question.

In this work, we investigate the generation of ultrarelativistic vortex positrons and electrons via NBW scattering of a vortex γ photon in a circularly polarized (CP) laser [Fig. 1 (a)]. We develop the AM-resolved NBW scattering theory within the

* jianxing@xjtu.edu.cn

strong-field quantum electrodynamics (SF-QED) framework [51, 53, 76] while incorporating the AM of all participating particles: laser photons, vortex γ photon, and the generated leptons. We establish the vortex positron generation condition by examining the kinematics in momentum space, specifically by exploring the possibility of postselecting a plane-wave electron to generate a vortex positron. We find that vortex positrons arise upon postselecting electrons along the collision axis ($\mathbf{p}_{e^-} \parallel \hat{z}$), and this scenario can be optimized to yield a considerable probability. Under the condition $\mathbf{p}_{e^-} \parallel \hat{z}$, we derive the AM conservation relation and analyze impacts of multiphoton absorption and total SAM from scattering particles. We find that the OAM of the positron receives contributions from the γ photon OAM and is amplified by the AM of multiple laser photons. These findings also hold for the symmetric case: ultrarelativistic vortex electrons can be generated when the positron is created along the collision axis.

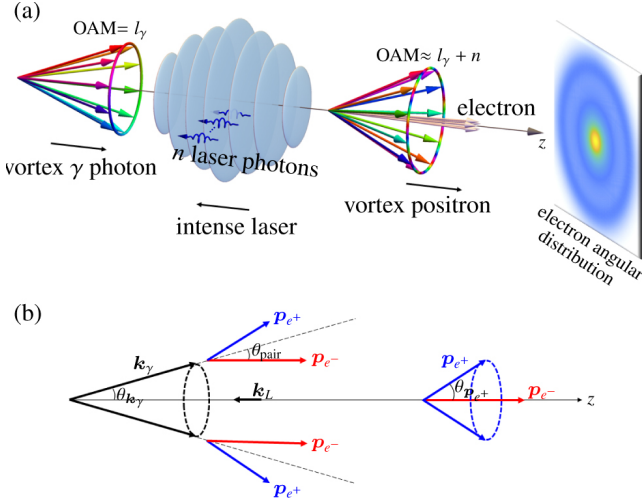


FIG. 1. (a) Generation of an ultrarelativistic vortex positron with large OAM via the NBW process. A vortex γ photon carrying OAM l_γ collides head-on with a CP laser and absorbs n laser photons, subsequently decaying into electron and positron pair. When the electron is postselected along the collision axis, the generated positron assumes a vortex state with OAM $l_\gamma + n$. The angular distribution exhibits a bright spot, indicating a maximum probability for electron creation along the collision axis. (b) The condition for producing a vortex positron illustrated in momentum space. The momentum vectors \mathbf{k}_γ , \mathbf{k}_L , \mathbf{p}_{e^-} , and \mathbf{p}_{e^+} correspond to the γ photon, laser photon, electron, and positron, respectively. θ_{k_γ} is the cone opening angle of the vortex state, $\theta_{p_{e^+}}$ is the polar angle of the momentum vector \mathbf{p}_{e^+} , and θ_{pair} is the NBW pair creation angle relative to the γ photon wave vector \mathbf{k}_γ .

Our paper is organized as follows: In Sec. II, we introduce basic considerations of NBW scattering of the vortex γ photon and establish the condition for the generation of vortex pairs. In Sec. III, we analyze the properties of the vortex pairs by presenting the theoretical framework for vortex positron generation and obtaining numerical results for the pair creation rates. We discuss the feasibility of our proposal and the detection of the vortex γ photon in Sec. IV. Finally, we end our

paper with a brief summary in Sec. V.

Throughout, natural units are used ($\hbar = c = 1$), the fine structure constant is $\alpha = \frac{e^2}{4\pi} \approx \frac{1}{137}$ with the electron charge $e = -|e|$, and the electron mass is denoted as m_e .

II. NBW SCATTERING OF THE VORTEX γ PHOTON

We consider the head-on collision between a vortex γ photon and a plane-wave laser pulse along the z axis [Fig. 1 (a)] and investigate the pair creation process by calculating the respective NBW scattering within the Furry picture of SF QED [51, 53, 76]. In the following, we first introduce our treatment of the incoming vortex γ photon and then establish the kinematic condition for obtaining final state vortex pairs.

A. Kinematic condition for the generation of vortex pairs

The vortex γ photon propagating along the z axis can be described by the Bessel wave packet in terms of the plane-wave function $A_\Lambda^\mu(t, \mathbf{r})$ as [27]

$$\mathcal{A}_{j_\gamma \Lambda}^\mu(t, \mathbf{r}) = \int \frac{d^2 \mathbf{k}_{\gamma, \perp}}{(2\pi)^2} a_{j_\gamma}(\mathbf{k}_{\gamma, \perp}) A_\Lambda^\mu(t, \mathbf{r}), \quad (1)$$

where Λ represents the helicity, j_γ is the total angular momentum (TAM), and the vortex amplitude $a_{j_\gamma}(\mathbf{k}_{\gamma, \perp})$ reads

$$a_j(\mathbf{k}_{\gamma, \perp}) = (-i)^j e^{i j \varphi_{k_\gamma}} \sqrt{\frac{2\pi}{k_{\gamma, \perp 0}}} \delta(|\mathbf{k}_{\gamma, \perp}| - k_{\gamma, \perp 0}). \quad (2)$$

The vortex amplitude encodes a cone structure with radius $|\mathbf{k}_{\gamma, \perp}| = k_{\gamma, \perp 0}$ in the momentum space featuring a helical phase factor $e^{i j \varphi_{k_\gamma}}$. In the illustration shown in Fig. 1, we represent a Bessel vortex particle using a cone with an opening angle in momentum space. In general, the Bessel mode wave function of the vortex particle $|\psi_{\text{vortex}}\rangle$ is expressed in terms of the plane-wave function $|\psi_{\text{plane}}\rangle$ by employing the vortex amplitude in Eq. (2) as $|\psi_{\text{vortex}}\rangle = \int \frac{d^2 \mathbf{p}_\perp}{(2\pi)^2} a_j(\mathbf{p}_\perp) |\psi_{\text{plane}}\rangle$. Bessel modes represent the simplest kink of vortex modes and allow for detailed calculations while reflecting key physics aspects related to AM transfer mechanism properly. The generation of vortex pairs involves obtaining similar wave packet structures for final states during NBW scattering.

The condition for generating the vortex positron and electron is determined through the following argument in momentum space [Fig. 1 (b)]. The momentum vectors \mathbf{k}_γ of the constituent plane waves in a vortex photon exhibit a conical distribution characterized by an opening angle θ_{k_γ} given by $\theta_{k_\gamma} = \arcsin(|\mathbf{k}_{\gamma, \perp}|/|\mathbf{k}_\gamma|)$, where $\mathbf{k}_{\gamma, \perp}$ is the transverse component of the momentum \mathbf{k}_γ [27]. A generated positron can be identified as a Bessel mode vortex particle when it exhibits

a similar conical structure in momentum space [77, 78]. For each momentum vector \mathbf{k}_γ , the generated electron-positron pair possesses an angle θ_{pair} with respect to the propagation direction of the plane-wave component. Under the condition $\theta_{\text{pair}} = \theta_{\mathbf{k}_\gamma}$, the plane-wave electron is produced along the collision axis, with a zero polar angle with respect to this axis ($\theta_{\mathbf{p}_{e^-}} = 0$), and the momentum vector \mathbf{p}_{e^+} of the plane-wave positron is uniquely determined, exhibiting a fixed polar angle $\theta_{\mathbf{p}_{e^+}}$. As the wave vector \mathbf{k}_γ traverses the cone, the momentum \mathbf{p}_{e^+} of the positron also spreads out over a cone with an opening angle $\theta_{\mathbf{p}_{e^+}}$, thereby indicating its vortex state. Note that the polar angle $\theta_{\mathbf{p}_{e^-}}$ could take a very small, nonzero value, and the vortex positron can be generated as long as the electron's azimuthal angle $\varphi_{\mathbf{p}_{e^-}}$ remains undetermined (see Appendixes A and B). These arguments also apply to the symmetric case. When the positron is created along collision axis ($\theta_{\mathbf{p}_{e^+}} = 0$), the electron momentum \mathbf{p}_{e^-} lies on a cone, resulting in the generation of a vortex electron. In the following, we continue our exploration of vortex positron generation.

B. Angular distribution of the created pairs

As postselection of an electron along the collision axis is critical for vortex positron generation, we examine the angle-resolved probability distribution of the created pairs. The NBW scattering of the vortex γ photon takes place in a CP plane-wave field,

$$A^\mu(\phi = k_L \cdot x) = a g(\phi) \begin{pmatrix} 0 \\ \cos \phi \\ \sin \phi \\ 0 \end{pmatrix}, \quad (3)$$

where k_L denotes the momentum four-vector of the laser photon, $a = a_0 m_e / e$ is the normalized vector potential with the dimensionless parameter a_0 , and $g(\phi)$ denotes the pulse shape function. The S -matrix element for the creation of plane-wave pairs from the vortex γ photon during NBW processes ($\gamma_{\text{vortex}} + n \omega_L \rightarrow e_{\text{plane wave}}^+ + e_{\text{plane wave}}^-$) can be expressed as

$$S_{fi}^{\text{1vortex}} = \int \frac{d^2 \mathbf{k}_{\gamma,\perp}}{(2\pi)^2} a_{j_\gamma}(\mathbf{k}_{\gamma,\perp}) S_{fi}^{\text{plane}}, \quad (4)$$

where S_{fi}^{plane} is the usual NBW S -matrix element with plane-wave particles [53]. The corresponding pair creation probability in terms of the electron's energy ε_{e^-} and solid angle Ω_{e^-} is

$$\frac{d^2 W^{\text{1vortex}}}{d\varepsilon_{e^-} d\Omega_{e^-}} = \int \frac{d\varphi_{\mathbf{k}_\gamma}}{2\pi} \frac{d^2 W^{\text{plane}}(\theta_{\mathbf{k}_\gamma}, \varphi_{\mathbf{k}_\gamma})}{d\varepsilon_{e^-} d\Omega_{e^-}}, \quad (5)$$

where $\frac{d^2 W^{\text{plane}}(\theta_{\mathbf{k}_\gamma}, \varphi_{\mathbf{k}_\gamma})}{d\varepsilon_{e^-} d\Omega_{e^-}}$ is the usual NBW pair creation probability for plane-wave particles in pulsed lasers [79, 80]. The angle-differential probability $dW^{\text{1vortex}}/d\Omega_{e^-}$ is obtained by integrating out the energy.

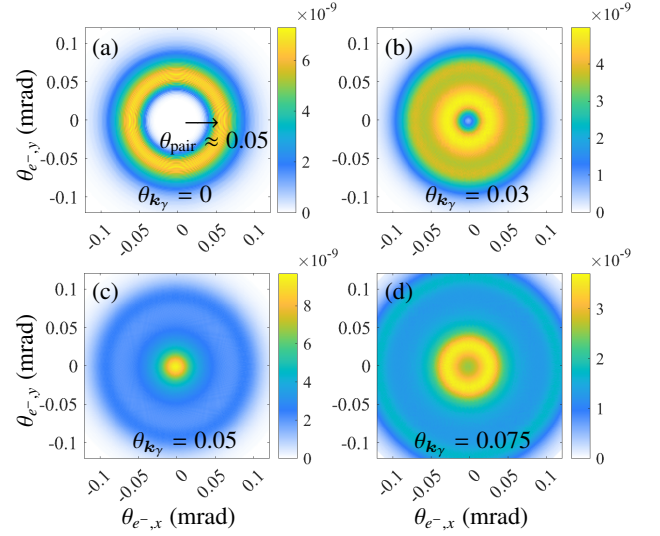


FIG. 2. The probability distribution $dW^{\text{1vortex}}/d\Omega_{e^-}$ of the electron in $\theta_{e-x}, \theta_{e-y}$ plane corresponding to NBW scattering in CP lasers with (a) the plane-wave γ photon and (b)-(d) the vortex state γ photons with different cone opening angles $\theta_{\mathbf{k}_\gamma}$. $\theta_{\mathbf{k}_\gamma}$ is the vortex γ photon's cone opening angle. $\theta_{\mathbf{k}_\gamma} = 0$ corresponds to the case of plane-wave γ photon scattering with the laser along the collision axis.

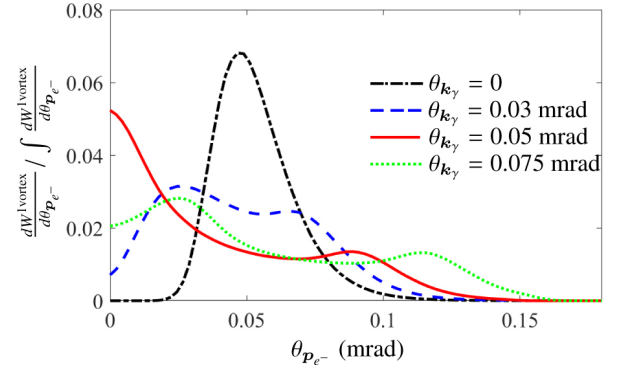


FIG. 3. Normalized probability distribution vs electron's propagation angle $\theta_{\mathbf{p}_{e^-}}$ with respect to the collision axis. The distribution is normalized by the total probability $\int \frac{dW^{\text{1vortex}}}{d\theta_{\mathbf{p}_{e^-}}}$ and presented with the resolution $\Delta\theta_{\mathbf{p}_{e^-}} \approx 0.002$ mrad.

In Fig. 2, we present the probability distribution $dW^{\text{1vortex}}/d\Omega_{e^-}$ of the created electron in the $\theta_{e-x}, \theta_{e-y}$ plane, obtained by using Eq. (5), where we define $d\Omega_{e^-} = d\theta_{e-x} d\theta_{e-y}$. We set laser intensity to $a_0 = 1$ and employ the pulse shape function $g(\phi) = \sin^2(\frac{\phi}{2N_{\text{cycle}}})$, where the number of laser pulse cycles is set as $N_{\text{cycle}} = 8$, and the central laser frequency is $\omega_L = 1.55$ eV. The energy of the vortex γ photon is set to $\varepsilon_\gamma = 20$ GeV, and calculations are conducted for various values of $\theta_{\mathbf{k}_\gamma}$. When electron-positron pairs are created from plane-wave γ photons ($\theta_{\mathbf{k}_\gamma} = 0$), the angle distribution features a ring with radius $\theta_{\text{pair}} \approx 0.05$ mrad [Fig. 2 (a)]. Here, $\theta_{\text{pair}} \sim a_0 m_e / \varepsilon_\gamma$ is the NBW pair creation angle with the maximum probability. When the vortex γ photon is

considered, the results depend on the relation between θ_{k_γ} and θ_{pair} , as shown in Figs. 2 (b)-2(d). In particular, when $\theta_{\text{pair}} = \theta_{k_\gamma}$ [Fig. 2 (c)], there is a peak at the center of the angle-resolved probability distribution, which favors the special condition $\theta_{p_{e^-}} = 0$ for the generation of the vortex positron.

In Fig. 3, we display the redefined angle-resolved result ($dW/d\theta_{p_{e^-}}$) from Fig. 2 for direct comparison of results obtained for different θ_{k_γ} , where we introduce $\theta_{p_{e^-}} = \sqrt{\theta_{e^-,x}^2 + \theta_{e^-,y}^2}$. The electrons generated along the collision axis fall within the angular range $0 \leq \theta_{p_{e^-}} \leq 0.002$ mrad ($0 \leq \theta_{p_{e^-}} \leq 0.005$ mrad), constituting 5.2% (11.6%) of the total electron yield, as illustrated by the solid red line in Fig. 3. In the plane-wave limit of the γ photon ($\theta_{k_\gamma} = 0$), the electron emerges predominantly at an angle of $\theta_{p_{e^-}} \approx 0.05$ mrad relative to the collision axis, as evidenced by the peak position of the dot-dashed black line in Fig. 3. Therefore, optimizing the probability for electron generation along the collision axis occurs when the cone opening angle of the vortex γ photon aligns with the dominant pair creation angle associated with the plane-wave component of the γ photon.

III. PROPERTIES OF THE GENERATED VORTEX PAIRS

We obtain the vortex positron generation probability and elucidate the AM transfer mechanism by applying the kinematic condition $\theta_{p_{e^-}} = 0$, which leads to the generation of vortex positrons and yields the maximum probability, as discussed in the previous section. To this end, we develop an AM-resolved NBW scattering theory and numerically investigate the energy and OAM distribution properties of the generated vortex positron.

A. Theoretical considerations

1. The AM-resolved NBW scattering theory

To fully understand the AM transfer mechanism in NBW scattering, it is essential to take into account both the SAM and OAM contributions from all the particles involved. The harmonic expansion of the scattering amplitude is carried out to account for the SAM contribution resulting from multiple laser photon absorption in a CP laser. In the pulsed laser case, the harmonic expansion is possible via the slowly varying envelope approximation (SVEA) [81] assuming that the laser pulse is long enough ($N_{\text{cycle}} \gg 1$) or that the pulse shape function is slowly varying [$\frac{\partial}{\partial \phi} g(\phi) \ll g(\phi)$]. After applying SVEA relations such as $\int d\phi g(\phi) \sin(\phi) \approx -g(\phi) \cos(\phi)$ and $\int d\phi g(\phi) \cos(\phi) \approx g(\phi) \sin(\phi)$, one can perform the harmonic expansion using the Jacobi-Anger type expansion

$$e^{i\alpha g(\phi) \sin(\phi + \varphi_p)} = \sum_n J_n(\alpha g(\phi)) e^{in(\phi + \varphi_p)}, \quad (6)$$

where J_n is the Bessel function of the first kind. In this context, ϕ represents the laser phase, whereas φ_p denotes the azimuthal angle of the electron/positron's momentum.

Regarding the numerical calculations in our work, it is observed that the use of the SVEA provides a satisfactory approximation, even for $N_{\text{cycle}} = 6$, as demonstrated in Fig. 4. For the optical laser ($\omega_L = 1.55$ eV), this requirement translates to the laser pulse duration as, $\tau \geq 16$ fs. The SVEA applies more to increasing values of N_{cycle} .

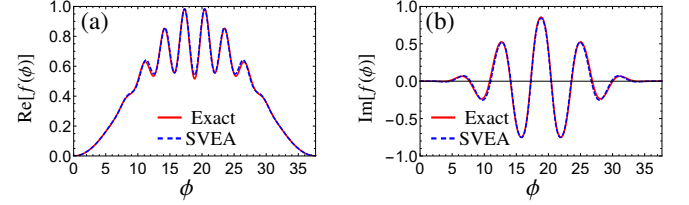


FIG. 4. Comparison of the exact result for $f(\phi) = g(\phi)e^{-i \int d\phi g(\phi) \sin \phi}$ (solid red curves) and the corresponding SVEA result (dashed blue curves), where real and imaginary parts are presented in (a) and (b), respectively. The pulse shape function is $g(\phi) = \sin^2(\frac{\phi}{2N_{\text{cycle}}})$ with $N_{\text{cycle}} = 6$.

The electron and positron spinors, denoted as $u_{s_{e^-}}$ and $v_{s_{e^+}}$ respectively, along with the polarization vector of the γ photon, denoted as ϵ_Λ , are expressed as expansions using the corresponding spin eigenfunctions

$$\begin{aligned} u_{s_{e^-}} &= \sum_{\sigma_{e^-} = \pm \frac{1}{2}} e^{-i\sigma_{e^-}\varphi_{p_{e^-}}} d_{\sigma_{e^-}, s_{e^-}}^{1/2}(\theta_{p_{e^-}}) \begin{pmatrix} \sqrt{\varepsilon_{e^-} + m_e} w_z^{\sigma_{e^-}} \\ 2s_{e^-} \sqrt{\varepsilon_{e^-} - m_e} \tilde{w}_z^{\sigma_{e^-}} \end{pmatrix}, \\ v_{s_{e^+}} &= \sum_{\sigma_{e^+} = \pm \frac{1}{2}} e^{i\sigma_{e^+}\varphi_{p_{e^+}}} d_{\sigma_{e^+}, s_{e^+}}^{1/2}(\theta_{p_{e^+}}) \begin{pmatrix} -2s_{e^+} \sqrt{\varepsilon_{e^+} - m_e} \tilde{w}_z^{\sigma_{e^+}} \\ \sqrt{\varepsilon_{e^+} + m_e} \tilde{w}_z^{\sigma_{e^+}} \end{pmatrix}, \quad (7) \\ \epsilon_\Lambda &= \sum_{\sigma_\gamma = 0, \pm 1} e^{-i\sigma_\gamma \varphi_{k_\gamma}} d_{\sigma_\gamma, \Lambda}^1(\theta_{k_\gamma}) \chi_{\sigma_\gamma}, \end{aligned}$$

where ε_{e^-} (ε_{e^+}) is the electron (positron) energy. The variables $\varphi_{p_{e^-}}$, $\theta_{p_{e^-}}$, $\varphi_{p_{e^+}}$, $\theta_{p_{e^+}}$, φ_{k_γ} , and θ_{k_γ} represent the azimuthal and polar angles of the electron (p_{e^-}), positron (p_{e^+}), and γ photon (k_γ) momentum vectors, respectively. The spin eigenfunctions in Eq. (7) satisfy $\hat{s}_z w_z^{\sigma_{e^-}} = \sigma_{e^-} w_z^{\sigma_{e^-}}$ and $\hat{s}_z \chi_{\sigma_\gamma} = \sigma_\gamma \chi_{\sigma_\gamma}$, with the corresponding eigenvalues $\sigma_{e^-} = \pm 1/2$ and $\sigma_\gamma = \pm 1, 0$, respectively. The corresponding SAM are denoted by s_{e^-} , s_{e^+} , and Λ . The spinors are given by $w_z^{1/2} = (1, 0)^T$ and $w_z^{-1/2} = (0, 1)^T$, and the vectors are given by $\chi_0 = (0, 0, 1)^T$ and $\chi_\pm = \frac{\mp i}{\sqrt{2}}(1, \pm i, 0)^T$. The corresponding spin operators in the z direction, \hat{s}_z , are a 2×2 Pauli matrix $\hat{s}_z = \frac{1}{2}\hat{\sigma}_z$ for the spinor and a 3×3 spin-1 matrix for the vector [82]. The spinors for the electron and the positron satisfy the relation $\tilde{w}_z^\pm = \pm w_z^\mp$. The Wigner's d functions are

$$d_{\sigma, s}^{1/2}(\theta) = \begin{pmatrix} \cos \theta/2 & -\sin \theta/2 \\ \sin \theta/2 & \cos \theta/2 \end{pmatrix}, \quad (8)$$

and

$$d_{\sigma,\Lambda}^1(\theta) = \begin{pmatrix} \cos^2 \theta/2 & -\frac{1}{\sqrt{2}} \sin \theta & \sin^2 \theta/2 \\ \frac{1}{\sqrt{2}} \sin \theta & \cos \theta & -\frac{1}{\sqrt{2}} \sin \theta \\ \sin^2 \theta/2 & \frac{1}{\sqrt{2}} \sin \theta & \cos^2 \theta/2 \end{pmatrix}. \quad (9)$$

The explicit calculation of the AM transfer relation during NBW scattering involves coupling the phase factors that depend on the azimuth angle φ and encode SAM and OAM contributions of the corresponding particles, in Eqs. (2), (6), and (7). For the kinematic scenario of $\theta_{p_e^-} = 0$ [illustrated in Fig. 1 (b)], the scattering process exhibits rotational symmetry in the transverse plane, and the azimuthal angle dependent phase factors turn into a delta function that represents AM conservation. In the following, we obtain the AM-resolved NBW scattering amplitude and probability distributions using the previously introduced definitions.

2. Probability for the detection of vortex positron

The S -matrix element for the generation of vortex positron from the vortex γ photon ($\gamma_{\text{vortex}} + n\omega_L \rightarrow e_{\text{vortex}}^+ + e_{\text{plane wave}}^-$) can be expressed as

$$\begin{aligned} S_{fi}^{2\text{vortex}} &= \int \frac{d^2 \mathbf{k}_{\gamma,\perp}}{(2\pi)^2} \frac{d^2 \mathbf{p}_{e^+,\perp}}{(2\pi)^2} a_{j_\gamma}(\mathbf{k}_{\gamma,\perp}) a_{j_{e^+}}^*(\mathbf{p}_{e^+,\perp}) S_{fi}^{\text{plane}} \\ &= \frac{ie(2\pi)}{\omega_L} \delta(k_{\gamma,z} + sk_{L,z} - p_{e^-,z} - p_{e^+,z}) \delta(p_{\perp 0} - k_{\perp 0}) \\ &\quad \times \sum_n i^{j_\gamma + j_{e^+}} \delta_{j_\gamma + n, j_{e^+} + s_{e^-}} \mathcal{M}_n(s), \end{aligned} \quad (10)$$

where $a_{j_\gamma}(\mathbf{k}_{\gamma,\perp})$ and $a_{j_{e^+}}^*(\mathbf{p}_{e^+,\perp})$ denote vortex amplitudes of the vortex γ photon (with TAM j_γ) and the vortex positron (with TAM j_{e^+}), respectively. The quantity $s = \frac{k_\gamma p_{e^+}}{k_L(k_\gamma - p_{e^+})}$ is the continues laser photon absorption number obtained from the energy-momentum conservation relation. In Eq. (10), we project the final states onto a plane-wave electron and a vortex positron, which amounts to postselecting a plane-wave electron and detecting the vortex positron. Upon postselecting the electron alone would result in the generation of vortex positrons in a superposition of different OAM modes, as shown in Eq. (B1) in Appendix B. The spin and helicity dependent probability for detecting vortex positrons with energy ε_{e^+} is given by

$$\frac{dW^{2\text{vortex}}}{d\varepsilon_{e^+}} = \frac{\alpha}{4\varepsilon_\gamma} \frac{\varepsilon_{e^+} p_{e^+,z}}{(k_L p_{e^-})(k_L p_{e^+})} \sum_n \delta_{j_\gamma + n, j_{e^+} + s_{e^-}} |\mathcal{M}_n(s)|^2, \quad (11)$$

where we assume the special condition for the electron's polar angle $\theta_{p_e^-} = 0$. The amplitude \mathcal{M}_n is given by

$$\begin{aligned} \mathcal{M}_n &= \\ &d_{s_{e^+}, s_{e^-}}^{1/2}(\theta_1) d_{2s_{e^-}, \Lambda}^1(\theta_k) (-\sqrt{2}) f^{(2)} \mathcal{C}_0^{(n)}(s) - d_{-s_{e^+}, s_{e^-}}^{1/2}(\theta_1) d_{0, \Lambda}^1(\theta_k) \\ &\quad \times [f^{(2)} \mathcal{C}_0^{(n)}(s) + 2\alpha_{e^-} \alpha_{e^+} (-2s_{e^+} f^{(1)} + f^{(2)}) \mathcal{C}_2^{(n)}(s) + \\ &\quad \mathcal{C}_{2s_{e^+}}^{(n)}(s) \{d_{s_{e^+}, s_{e^-}}^{1/2}(\theta_1) d_{0, \Lambda}^1(\theta_k) [\alpha_{e^-} (f^{(1)} + 2s_{e^+} f^{(2)}) + \\ &\quad \alpha_{e^+} (f^{(1)} - 2s_{e^-} f^{(2)})] + \\ &\quad d_{-s_{e^+}, s_{e^-}}^{1/2}(\theta_1) d_{-2s_{e^+}, \Lambda}^1(\theta_k) \sqrt{2} \alpha_{e^+} (f^{(1)} - 2s_{e^+} f^{(2)})\} + \\ &\quad \mathcal{C}_{-2s_{e^+}}^{(n)}(s) d_{-s_{e^+}, s_{e^-}}^{1/2}(\theta_1) d_{2s_{e^+}, \Lambda}^1(\theta_k) \sqrt{2} \alpha_{e^-} (f^{(1)} - 2s_{e^+} f^{(2)})]. \end{aligned} \quad (12)$$

For better readability, we use θ_1 and θ_k as short notations for $\theta_{p_{e^+}}$ and θ_{k_γ} , respectively. The following definitions are used:

$$\begin{aligned} f^{(1)} &= 2s_{e^-} \sqrt{\varepsilon_{e^-} - m_e} \sqrt{\varepsilon_{e^+} + m_e} - 2s_{e^+} \sqrt{\varepsilon_{e^-} + m_e} \sqrt{\varepsilon_{e^+} - m_e}, \\ f^{(2)} &= \sqrt{\varepsilon_{e^-} + m_e} \sqrt{\varepsilon_{e^+} + m_e} + 2s_{e^-} (-2s_{e^+}) \sqrt{\varepsilon_{e^-} - m_e} \sqrt{\varepsilon_{e^+} - m_e}, \end{aligned}$$

and the dynamic integrals are

$$\begin{aligned} \mathcal{C}_0^{(n)}(s) &= \int d\phi e^{i(s-n)\phi - i(\beta_{e^-} + \beta_{e^+})} \int^\phi d\phi' g^2(\phi') J_n(\alpha_{p_{e^+}} g(\phi)), \\ \mathcal{C}_2^{(n)}(s) &= \int d\phi e^{i(s-n)\phi - i(\beta_{e^-} + \beta_{e^+})} \int^\phi d\phi' g^2(\phi') g^2(\phi) J_n(\alpha_{p_{e^+}} g(\phi)), \\ \mathcal{C}_{\sigma=\pm}^{(n)}(s) &= \int d\phi e^{i(s-n)\phi - i(\beta_{e^-} + \beta_{e^+})} \int^\phi d\phi' g^2(\phi') g(\phi) J_{n-\sigma}(\alpha_{p_{e^+}} g(\phi)), \end{aligned}$$

with the kinematic factors defined as

$$\alpha_{p_{e^+}} = \frac{m_e p_{e^+,\perp}}{k_L p_{e^+}} a_0, \quad \alpha_{e^-/e^+} = \frac{m_e \omega_L}{k_L p_{e^-/e^+}} a_0, \quad \beta_{e^-/e^+} = \frac{m_e^2 a_0^2}{2k_L p_{e^-/e^+}}.$$

In Eq. (11), the interference term $\sum_{n \neq n'} \mathcal{M}_n \mathcal{M}_{n'}^*$ is eliminated by the AM conserving δ function, which enables one to express the TAM of the created vortex positron as $j_{e^+} = j_\gamma + n - s_{e^-}$. Thus, the vortex positron receives AM contributions from the γ photon (j_γ), the multiple laser photons (n), and the SAM of the electron (s_{e^-}). Here, laser photons impart extra AM into the scattering process, enhancing the contribution from the vortex γ photon j_γ by n . Therefore, higher particle yield, plane-wave postselection criteria, and AM enhancement via multiphoton absorption, facilitated by the intense laser, distinguish our results from linear scattering processes [43–45].

B. Numerical results

The energy spectrum of the vortex positron is determined numerically by utilizing Eq. (11). We display the results for a vortex γ photon with cone opening angle of $\theta_{k_\gamma} = 0.05$ mrad while employing the same parameters as in Fig. 2. After examining a broad spectrum of harmonics spanning from 1 to 80, we found that the most significant contributions come from those within the range $10 \leq n \leq 40$. The cumulative

effect of all other harmonics outside this range is at least 4 orders of magnitude smaller. To better demonstrate the OAM distribution, the range of the plots has been made smaller and now includes only the interval $12 \leq n \leq 35$. We find that the dominant contribution comes from harmonics in the range $10 \leq n \leq 35$. As shown in Fig. 5 (a), the vortex positron is produced with a broad energy spectrum due to intense laser pulses. Given the relation $|\mathbf{p}_{e^+, \perp}| = |\mathbf{k}_{\gamma, \perp}|$, the energy of the vortex positron ε_{e^+} and its cone opening angle $\theta_{p_{e^+}} = \arcsin |\mathbf{p}_{e^+, \perp}|/|\mathbf{p}_{e^+}|$ satisfy $\varepsilon_{e^+} \approx |\mathbf{k}_{\gamma, \perp}|/\theta_{p_{e^+}}$ [the dashed red line in Fig. 5 (a)]. Moreover, considering the kinematic condition $\theta_{p_{e^-}} = 0$, specifying the energy ε_{e^+} of the positron uniquely determines its polar angle $\theta_{p_{e^+}}$, thereby defining a conical shape in momentum space. The remaining aspect to be characterized is its AM property.

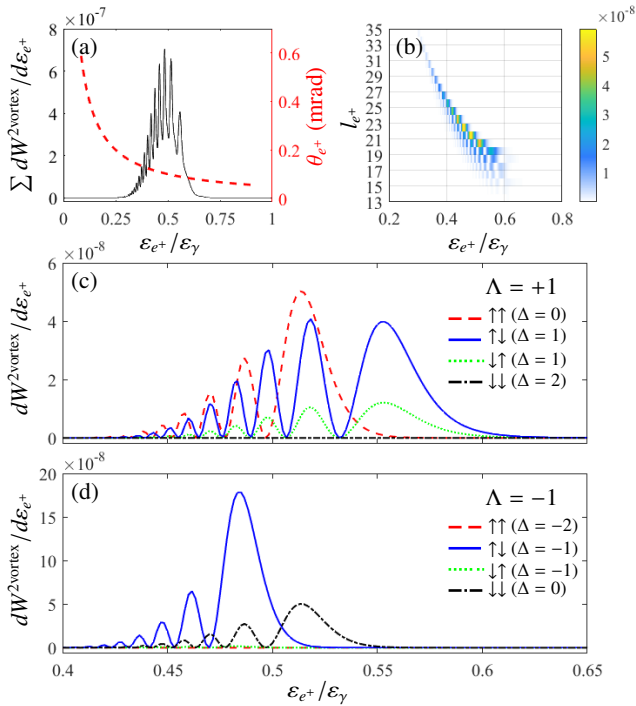


FIG. 5. (a) Solid black line: the probability distribution of the vortex positron generation with respect to the energy ratio $\varepsilon_{e^+}/\varepsilon_\gamma$. The probability is summed for NBW harmonics and particle spins. Dashed red line: the vortex positron's cone opening angle $\theta_{p_{e^+}}$ vs the energy ratio $\varepsilon_{e^+}/\varepsilon_\gamma$. (b) The probability distribution of the vortex positron generation with respect to OAM l_{e^+} and the energy ratio $\varepsilon_{e^+}/\varepsilon_\gamma$ for helicity $\Lambda = 1$ and spins $s_{e^-} = s_{e^+} = 1/2$. (c),(d): Probability distributions of the vortex positron generation with respect to the energy ratio $\varepsilon_{e^+}/\varepsilon_\gamma$ for the fixed $l_{e^+} = 20$ for the γ photon helicities $\Lambda = +1$ and $\Lambda = -1$, respectively. The arrows on the left (right) represent the electron (positron) spin states, with \uparrow and \downarrow denoting $s_{e^-/e^+} = \frac{1}{2}$ and $s_{e^-/e^+} = -\frac{1}{2}$, respectively. The spin contributions from scattering particles are defined as $\Delta = \Lambda - s_{e^-} - s_{e^+}$.

Both the AM of the absorbed laser photons and the spin contributions from the scattering particles play significant roles in determining the AM of the vortex positron. In our collision scenario, with particle energies in the multi-GeV

range and transverse momenta below a few MeV, the paraxial approximation holds, rendering the intrinsic spin-orbit interaction associated with the vortex particle negligible. Consequently, the TAM of the vortex particle can be decomposed into the SAM and OAM [13, 83]. The OAM of the vortex γ photon is given by $l_\gamma = j_\gamma - \Lambda$, while that of the vortex positron is $l_{e^+} = j_{e^+} - s_{e^+}$, which results in the relation $l_{e^+} = l_\gamma + n + \Delta$, with $\Delta = \Lambda - s_{e^-} - s_{e^+}$. According to Eq. (11), the generation probability of vortex positrons involves incoherent summations over various combinations of spin and helicity, as well as different harmonic orders. For a given OAM $l_\gamma = 1$ and specific helicity ($\Lambda = 1$) and spin ($s_{e^-} = s_{e^+} = 1/2$) configurations, the positron OAM $l_{e^+} = 1 + n$ is uniquely determined for each harmonic n [Fig. 5 (b)]. Here, the n th harmonic contributes an AM number of n to the positron. Various spin and helicity configurations of the NBW process contribute to the same OAM value of the vortex positron. In this scenario, Δ encapsulates spin contributions from scattering particles and assumes integer values within the range $-2 \leq \Delta \leq 2$. In Figs. 5 (c) and 5(d), the pair creation rates for eight distinct spin configurations are depicted for $l_{e^+} = 20$. Among these, two configurations are significantly suppressed, and they correspond to $\Delta = \pm 2$. Consequently, the contributing values of Δ are limited to $\{-1, 0, 1\}$. Given that a substantial number of laser photons ($n \gg \Delta$) participate in the pair creation process, the OAM of the vortex positron arises from a transfer of OAM from the initial γ photon and the AM of multiple laser photons, leading to $l_{e^+} \approx l_\gamma + n$.

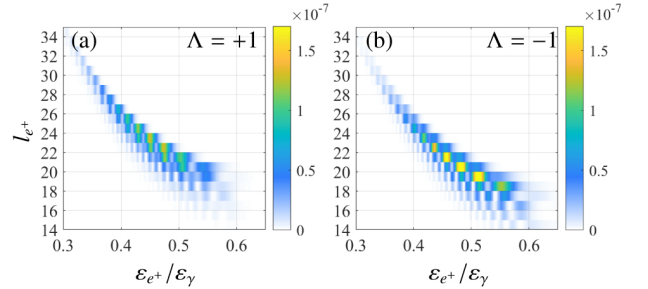


FIG. 6. The probability distribution of the vortex positron generation with respect to the positron's OAM and the energy ratio $\varepsilon_{e^+}/\varepsilon_\gamma$. The γ photon carries OAM $l_\gamma = 1$ and its helicity takes the values (a) $\Lambda = +1$ and (b) $\Lambda = -1$. The same set of γ photon and laser pulse parameters is used as in Fig. 5.

The OAM- and energy-resolved probability distributions for the generated vortex positron are presented in Fig. 6. Given the specified parameters $\omega_L = 1.55$ eV and $\omega = 20$ GeV, it is estimated that the number of absorbed laser photons exceeds $n \gtrsim 17$. As a result, even when the initial γ photon has $l_\gamma = 1$, the resulting positron attains a substantial OAM (Fig. 6). Upon comparing the results in Figs. 6 (a) and 6(b), it becomes apparent that the vortex γ photon with negative helicity ($\Lambda = -1$) is more favorable, exhibiting a relatively higher probability than its positive helicity counterpart. Notably, the OAM of the γ photon and AM of the multiple laser photons are transferred solely to the positron, leaving the electron as a plane-wave

particle. This scenario differs from NBW pair creation processes involving extrinsic OAM, where both the electron and the positron acquire the same amount of AM [72–75].

IV. DISCUSSION

A. Collision of the vortex γ photon with the intense laser

Considering the experimental feasibility of our proposal, the on-axis scattering geometry presents significant challenges both from an experimental standpoint and in terms of measuring the final particles. For scenarios involving on-axis or minimally angled scattering of the final electron, the magnitudes of the transverse momenta of involved particles adhere to relations such that $|\mathbf{k}_{\gamma,\perp}| \approx |\mathbf{p}_{e^+,\perp}| \lesssim 1 \text{ MeV} \gg |\mathbf{p}_{e^-,\perp}|$. Assuming typical particle energies in the GeV range, the implied polar angles are $\theta_\gamma \approx \theta_{e^+} \lesssim 1 \text{ mrad}$ and $\theta_{e^-} \ll 1 \text{ mrad}$. Consequently, experimentally discerning the produced vortex leptons becomes exceedingly challenging due to these minute angular separations. Concerning the assumption of an incoming vortex γ photon, there are theoretical proposals showing the possibility of producing vortex γ photons via Compton scattering processes [27, 84–88]. The pair creation setup is considered for the multiphoton regime ($a_0 \gtrsim 1$) [89, 90], with γ photon energies typically ranging around $\varepsilon_\gamma \sim \text{GeV}$. These parameters align with those used in the E144 experiment [89] and are also in line with those planned for upcoming experimental setups [91–93].

For GeV photons, the energy resolution of the operating Compton- γ sources has already reached $\frac{\Delta\varepsilon_\gamma}{\varepsilon_\gamma} \lesssim 1.25\%$ [94, 95]. In linear Compton sources, γ photons are predominantly generated along the scattering axis with the energy $\varepsilon_\gamma \approx 4\gamma_e^2\omega_L$ and the angular spread $\Delta\theta \lesssim \frac{1}{\gamma_e^2}$, where γ_e is the electron Lorentz factor [27, 86]. Moreover, nonlinear Compton sources with intense laser pulses can offer higher brilliance exceeding $10^{21} \text{ photons s}^{-1} \text{ mm}^{-2} \text{ mrad}^{-2} 0.1\% \text{ BW}$ at the cost of energy and divergence broadening due to multiphoton absorption and quantum stochasticity effects [53, 96], which may be narrowed by chirping [97, 98]. In theory, pair creation is also feasible using γ photons of lower energies. To achieve this, one could either increase the laser intensity (thus increasing the value of a_0) or employ lasers with higher frequencies, such as free-electron laser/x-ray free-electron laser pulses, to achieve substantial quantum nonlinearity parameter $\chi = a_0 \frac{2\omega_L\varepsilon_\gamma}{m_e^2} [53]$. However, it is crucial to note that employing ultraintense lasers ($a_0 \gg 1$) may initiate multiple radiation emissions and pair creations. These complex events must be carefully considered in the context of vortex particle scattering and could be the subject of separate, focused investigations.

Concerning the results for the vortex positron's energy and OAM distributions given in Figs. 5 and 6, we consider the NBW scattering of a single γ photon with a laser pulse. We present numerical results for a fixed set of parameters: a vortex γ photon energy $\varepsilon_\gamma = 20 \text{ GeV}$ and a cone opening

angle of $\theta_{\mathbf{k}_\gamma} = 0.05 \text{ mrad}$ (corresponding to $k_{\gamma,\perp} = 1 \text{ MeV}$). A spread in γ photon energy would alter the numerical results by producing distinct energy and OAM distributions for each set of ε_γ and $\theta_{\mathbf{k}_\gamma}$. However, the mechanism of vortex positron generation allows for variations in the energy spread. The key condition for vortex positron generation with maximum yield when postselecting an electron along the z axis is $\theta_{\text{pair}} = \theta_{\mathbf{k}_\gamma}$. Here, the typical pair creation angle is estimated as $\theta_{\text{pair}} \sim \frac{m_e a_0}{\varepsilon_\gamma}$, and the cone opening angle is given as $\theta_{\mathbf{k}_\gamma} = \frac{k_{\gamma,\perp}}{\varepsilon_\gamma}$. Thus, the condition translates into the relation $m_e a_0 \sim k_{\gamma,\perp}$, which imposes no specific restriction on the γ photon energy. However, a significant decrease in the γ photon energy would decrease the total pair creation probability while potentially increasing the number of absorbed laser photons.

B. Detection of the cone angle and the superposition states of the vortex γ photon

Beyond their intrinsic OAM, vortex particles exhibit distinctive transverse coherence that manifests in the form of a cone opening angle. This unique feature is anticipated to introduce novel kinematic aspects to scattering phenomena. In the context of our study, the cone opening angle $\theta_{\mathbf{k}_\gamma}$ of the vortex γ photon plays a pivotal role in optimizing the generation of vortex positrons, as exemplified in Fig. 3. We demonstrate the feasibility of detecting this angle by analyzing the created pairs' angular distribution during the NBW process. The pair creation probability in terms of the electron's energy ε_{e^-} and solid angle Ω_{e^-} is

$$\frac{d^2 W^{1\text{vortex}}}{d\varepsilon_{e^-} d\Omega_{e^-}} = \int \frac{d\varphi_{\mathbf{k}_\gamma}}{2\pi} F(\varphi_{\mathbf{k}_\gamma}) \frac{d^2 W^{\text{plane}}(\theta_{\mathbf{k}_\gamma}, \varphi_{\mathbf{k}_\gamma})}{d\varepsilon_{e^-} d\Omega_{e^-}}. \quad (13)$$

Here, $F(\varphi_{\mathbf{k}_\gamma})$ is related to the vortex state of the incoming γ photon such that $F(\varphi_{\mathbf{k}_\gamma}) = 1$ corresponds to the γ photon in the vortex eigenstate given by Eq. (5), and $F(\varphi_{\mathbf{k}_\gamma}) = 1 + \cos[\Delta j_\gamma(\varphi_{\mathbf{k}_\gamma} - \frac{\pi}{2}) + \delta]$ corresponds to the γ photon in the vortex superposition state ($\Delta j_\gamma = j_{\gamma,1} - j_{\gamma,2}$). The vortex amplitude of the superposition state is given as

$$\tilde{a}_{j_{\gamma,1}, j_{\gamma,2}}(\mathbf{k}_{\gamma,\perp}) = \frac{1}{\sqrt{2}} [a_{j_{\gamma,1}}(\mathbf{k}_{\gamma,\perp}) + e^{i\delta} a_{j_{\gamma,2}}(\mathbf{k}_{\gamma,\perp})]. \quad (14)$$

In our numerical calculations, we have set the relative phase factor to $\delta = 0$. This choice does not affect the conclusions drawn in our study, as varying δ merely induces a rotation of the angular distribution around the center of the $\theta_{e^-,x}\theta_{e^-,y}$ plane without altering its overall shape.

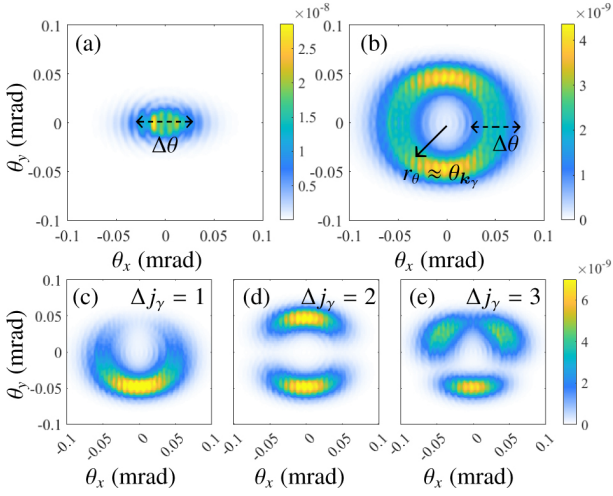


FIG. 7. The probability distribution $dW^{1\text{vortex}}(\theta_{k_\gamma})/d\Omega_{e^-}$ of the electron with respect to its propagation angle in the $\theta_{e-x}\theta_{e-y}$ plane during NBW scattering of the γ photon in LP lasers. The γ photon is in (a) a plane-wave state and (b) a vortex state. γ photons are in the vortex superposition states with $\Delta j_\gamma = 1, 2, \text{ and } 3$ in (c), (d), and (e), respectively.

The numerical results are obtained by using Eq. (5) for a linearly polarized (LP) laser pulse $A^\mu(\phi) = a g(\phi) \{0, \cos \phi, 0, 0\}$ with intensity $a_0 = 1$ for the same vortex γ photon parameter as in Fig. 5. When the incoming γ photon is in the plane-wave state ($\theta_{k_\gamma} = 0$), the created electron is concentrated at the center and exhibits a diameter $\Delta\theta$ that corresponds to the FWHM of the electron's angular distribution in the $\theta_{e-x}\theta_{e-y}$ plane [Fig. 7 (a)]. The vortex state of the γ photon causes the angular distribution of the electron to spread along a circle with radius r_θ and thickness $\Delta\theta$ [Fig. 7 (b)]. r_θ represents the radial distance from the center to the peak position of the probability distribution ring in the $\theta_{e-x}\theta_{e-y}$ plane. We observe that the radius of the electron angle distribution r_θ is closely related to the polar angle of the vortex γ photon $\theta_{k_\gamma} \approx r_\theta$; thus, one can discern the polar angle θ_{k_γ} by measuring r_θ . However, for the polar angle to be clearly resolved, the process should satisfy $r_\theta \geq \Delta\theta$; hence, one obtains the condition $\theta_{k_\gamma} \geq \Delta\theta$. When one estimates $\Delta\theta \sim a_0 m_e / \varepsilon_\gamma$ [79], the condition for effective measurement poses an upper limit on the laser intensity of $a_0 \lesssim |\mathbf{k}_{\gamma,\perp}|/m_e$.

Furthermore, when the vortex γ photon exists in a superposition state, e.g., with two distinct TAM values $j_{\gamma,1}$ and $j_{\gamma,2}$, as defined in Eq. (14)—a scenario possible in the generation of vortex γ photons via nonlinear Compton scattering in pulsed lasers [87, 88]—discrete patterns arise that are associated with the difference $\Delta j_\gamma = j_{\gamma,1} - j_{\gamma,2}$, which appears in the function $F(\varphi_{k_\gamma})$ in Eq. (13). In this case, the electron angle distribution can still reveal the polar angle θ_{k_γ} as pairs are created along the circle with radius $r_\theta \approx \theta_{k_\gamma}$ [Figs. 7 (c) and 7(d)].

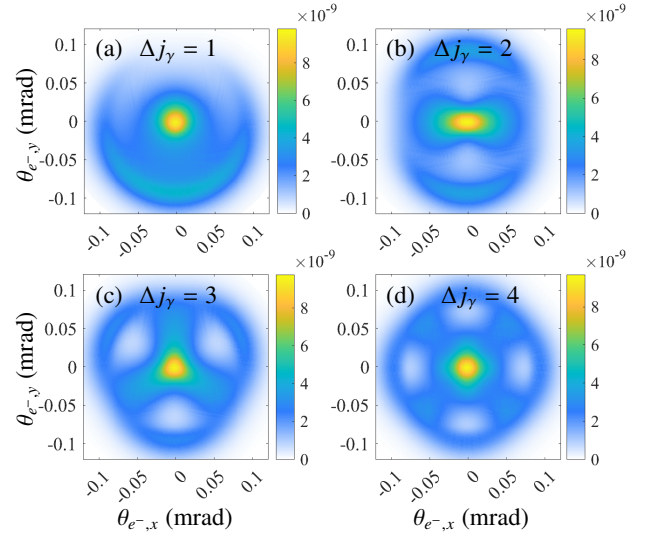


FIG. 8. The probability distribution $dW^{1\text{vortex}}/d\Omega_{e^-}$ of the electron in $\theta_{e-x}\theta_{e-y}$ plane corresponding to NBW scattering in CP lasers with a γ photon in the vortex superposition states with different Δj_γ values.

The probability distribution $dW^{1\text{vortex}}/d\Omega_{e^-}$ of the created electron in the $\theta_{e-x}\theta_{e-y}$ plane is shown in Fig. 8 for vortex superposition states of the γ photon in the CP laser case. Discrete patterns related to the value of Δj_γ arise in Fig. 8 as in the corresponding cases for a LP laser pulse in Figs. 7 (c) and 7(d). Comparing Figs. 2 and 8 for the CP laser to the corresponding results in Fig. 7 for the LP laser, we conclude that the LP laser case yields clearer signatures and is more suitable for detecting the cone opening angle θ_{k_γ} of the vortex γ photon.

V. CONCLUSION

In conclusion, we put forward a novel method of generating ultrarelativistic vortex positrons and electrons with large OAM through NBW scattering of vortex γ photon in CP lasers. We developed a complete AM-resolved quantum scattering theory and reveal the OAM-transfer mechanism of an NBW process. Our theoretical framework can be further developed to investigate vortex particle generation and detection in other SF-QED processes, and our findings also pave the way for the application of ultrarelativistic vortex leptons in high-energy particle physics, nuclear physics, astrophysics, etc.

ACKNOWLEDGMENTS The work is supported by the National Natural Science Foundation of China (Grants No.U2267204, No.12105217, and No.12147176), the Foundation of Science and Technology on Plasma Physics Laboratory (Grant No.JCKYS2021212008), the Natural Science Basic Research Program of Shaanxi (Grants No.2023-JC-QN-0091 and No.2024JC-YBQN-0042), and the Shaanxi Fundamental Science Research Project for Mathematics and Physics (Grants No. 22JSY014 and No.22JSQ019).

Appendix A: POSTSELECTING A BESSEL VORTEX ELECTRON

We begin by deriving the probability rate for the case where both the electron and positron are vortex particles. Subsequently, we calculate the result for the scenario where the electron is postselected in the zero-Bessel mode. The S matrix of the process ($\gamma_{\text{vortex}} + n \omega_L \rightarrow e_{\text{vortex}}^+ + e_{\text{vortex}}^-$) is written as

$$S_{fi}^{3\text{vortex}} = \int \frac{d^2 \mathbf{k}_{\gamma\perp}}{(2\pi)^2} \frac{d^2 \mathbf{p}_{1\perp}}{(2\pi)^2} \frac{d^2 \mathbf{p}_{2\perp}}{(2\pi)^2} \times a_{j_\gamma}(\mathbf{k}_{\gamma,\perp}) a_{j_1}^*(\mathbf{p}_{1,\perp}) a_{j_2}^*(\mathbf{p}_{2,\perp}) S_{fi}^{\text{pl}}, \quad (\text{A1})$$

where the initial γ photon, final electron, and positron are all vortex particles. As both of the final state particles in Eq. (A1) are projected onto the vortex modes, this corresponds to the assumption of postselecting the final electron (or positron) via a twisted detector as in [43–45]. The notations for the positron and electron are used as follows: $p_1 = p_{e^+}$, $p_2 = p_{e^-}$ for their momenta, and $j_1 = j_{e^+}$, $j_2 = j_{e^-}$ for their TAM. The pair creation rate reads

$$\frac{d^3 W}{dp_{1\perp} dp_{1z} dp_{2\perp}} = \frac{\pi e^2}{8} \frac{k_{\perp 0}}{(k_L p_1)(k_L p_2)} \left| \sum_{n_1, n_2} \delta_{j_\gamma + \Delta n, j_1 + j_2} \times \sum_{\sigma \dots} \frac{\cos(\Delta m_1 \delta_1 - \Delta m_2 \delta_2)}{p_{1\perp} p_{2\perp} \sin(\delta_1 + \delta_2)} \mathcal{M}_{n_1, n_2} \right|^2, \quad (\text{A2})$$

where the definitions of new symbols are $\Delta n = n_1 - n_2$, $\Delta m_{1/2} = j_{1/2} - \tilde{m}_{1/2}$, $\tilde{m}_1 = n_1 - \sigma + \sigma_1 - s_1$, $\tilde{m}_2 = -n_2 + \sigma_2 - s_2$, $\delta_1 = \arccos \frac{k_{\perp 0}^2 + p_{1\perp 0}^2 - p_{2\perp 0}^2}{2k_{\perp 0} p_{1\perp 0}}$, and $\delta_2 = \arccos \frac{k_{\perp 0}^2 - p_{1\perp 0}^2 + p_{2\perp 0}^2}{2k_{\perp 0} p_{2\perp 0}}$ [99]. In the second line of Eq. (A2), the summations over dummy indices $\{\sigma, \sigma_1, \sigma_2, \sigma_\gamma\}$ are performed. The harmonics are defined as follows:

$$\mathcal{M}_{n_1, n_2} = [\delta_{\sigma, 0} (\delta_{\sigma_1, \sigma_2} \mathcal{G}_0^{\uparrow\uparrow} + \delta_{\sigma_1, -\sigma_2} \mathcal{G}_0^{\uparrow\downarrow}) - (\delta_{\sigma_1, \sigma_2} \mathcal{G}_\pm^{\uparrow\uparrow} + \delta_{\sigma_1, -\sigma_2} \mathcal{G}_\pm^{\uparrow\downarrow})] d_{\sigma_1, s_1}^{1/2}(\theta_{\mathbf{p}_1}) d_{\sigma_2, s_2}^{1/2}(\theta_{\mathbf{p}_2}) d_{\sigma_\gamma, \Lambda}^1(\theta_{\mathbf{k}}), \quad (\text{A3})$$

with the following notations:

$$\begin{aligned} \mathcal{G}_0^{\uparrow\uparrow} &= \delta_{\sigma_\Lambda, 2\sigma_1} (-\sqrt{2}) f^{(2)} \mathcal{C}_0^{(n_1, n_2)}(s), \\ \mathcal{G}_0^{\uparrow\downarrow} &= \delta_{\sigma_\Lambda, 0} [f^{(2)} \mathcal{C}_0^{(n_1, n_2)}(s) \\ &\quad + 2\alpha_1 \alpha_2 (2\sigma_1 f^{(1)} + f^{(2)}) \mathcal{C}_2^{(n_1, n_2)}(s)], \\ \mathcal{G}_\pm^{\uparrow\uparrow} &= \delta_{\sigma, 2\sigma_1} \delta_{\sigma_\Lambda, 0} [\alpha_1 (f^{(1)} + 2\sigma_1 f^{(2)}) \\ &\quad + \alpha_2 (f^{(1)} - 2\sigma_1 f^{(2)})] \mathcal{C}_\sigma^{(n_1, n_2)}(s), \\ \mathcal{G}_\pm^{\uparrow\downarrow} &= [\delta_{\sigma, 2\sigma_1} \delta_{\sigma_\Lambda, -2\sigma_1} \sqrt{2} \alpha_1 (f^{(1)} + 2\sigma_1 f^{(2)}) \\ &\quad + \delta_{\sigma, -2\sigma_1} \delta_{\sigma_\Lambda, 2\sigma_1} \sqrt{2} \alpha_2 (f^{(1)} + 2\sigma_1 f^{(2)})] \mathcal{C}_\sigma^{(n_1, n_2)}(s). \end{aligned} \quad (\text{A4})$$

The dynamic integrals are written as follows:

$$\begin{aligned} \mathcal{C}_0^{(n_1, n_2)}(s) &= \int d\phi e^{i(s-\Delta n)\phi - i(\beta_1 + \beta_2)} \int^\phi d\phi' g^2(\phi') \\ &\quad \times J_{n_1}(\alpha_{p_1} g(\phi)) J_{n_2}(\alpha_{p_2} g(\phi)), \\ \mathcal{C}_2^{(n_1, n_2)}(s) &= \int d\phi e^{i(s-\Delta n)\phi - i(\beta_1 + \beta_2)} \int^\phi d\phi' g^2(\phi') \\ &\quad \times J_{n_1}(\alpha_{p_1} g(\phi)) J_{n_2}(\alpha_{p_2} g(\phi)) g^2(\phi), \\ \mathcal{C}_{\sigma=\pm}^{(n_1, n_2)}(s) &= \int d\phi e^{i(s-\Delta n)\phi - i(\beta_1 + \beta_2)} \int^\phi d\phi' g^2(\phi') \\ &\quad \times J_{n_1-\sigma}(\alpha_{p_1} g(\phi)) J_{n_2}(\alpha_{p_2} g(\phi)) g(\phi). \end{aligned} \quad (\text{A5})$$

In the main text, we assumed the zero scattering angle ($\theta_2 = 0$) for the electron and derived the AM conservation relations in Eqs. (10) and (11). To incorporate a more realistic scenario with a very small scattering angle $\theta_2 \rightarrow 0$, we consider postselecting an electron with vanishing transverse momentum and an undetermined azimuthal angle, which we model using a cone structure with a very small transverse momentum radius $p_{2\perp 0}$ that is akin to a zero-Bessel mode. For the case of an electron postselected with a zero-Bessel mode, we equate its TAM to its spin, $j_2 = s_2$, in Eq. (A2). Consequently, we recover the delta function $\delta_{j_\gamma + n, j_1 + s_2}$, which is the same as for the postselecting plane-wave electron along the collision axis, as given in Eq. (11). Furthermore, by postselecting electrons that meet the criterion of a small transverse momentum $|p_{2\perp}| \ll k_{\perp 0}$, the resulting vortex positron beam is also produced with a range of indefinite transverse momenta, thereby placing the beam in a mixed state configuration.

Appendix B: WAVE FUNCTION OF POSITRONS AFTER POSTSELECTING ELECTRONS ALONG THE SCATTERING AXIS

When the final electron is postselected into a zero-Bessel mode, the absolute value of its transverse momentum becomes fixed due to $\delta(|p_{2\perp}| - p_{2\perp 0})$, as evident from the vortex wave packet amplitude given by Eq. (2). Its azimuthal angle remains undetermined, a situation that is similar to a generalized measurement [31]. This type of generalized measurement is effectively realized when the transverse momentum is exceedingly small $p_{2\perp} \ll k_{\perp}$, making it practically impossible to measure the azimuthal angle φ_2 . This scenario aligns naturally with our assumption of electron scattering along the collision axis $\theta_2 \rightarrow 0$. Under these conditions, the wave function of the positron can be derived by computing the evolved state [31, 100],

$$\begin{aligned} |\psi_1^{\text{ev}}\rangle &= \int \frac{d^2 \mathbf{k}_{\gamma\perp}}{(2\pi)^2} \frac{d^2 \mathbf{p}_{2\perp}}{(2\pi)^2} a_{j_\gamma}(\mathbf{k}_{\gamma,\perp}) a_{j_2=0}^*(\mathbf{p}_{2,\perp}) v_{s_1} S_{fi}^{\text{plane}} \\ &= \frac{(-ie)}{\omega_L} \delta(k_{\gamma z} + s k_{Lz} - p_{1z} - p_{2z}) \sqrt{k_{\gamma\perp} p_{1\perp}} \delta(p_{1\perp} - p_{1\perp 0}) \\ &\quad \sum_{n_1, n_2, \sigma, \dots} (-i)^{j_\gamma} e^{-i(j_\gamma - \sigma_\Lambda + \tilde{m}_1 + \tilde{m}_2 + \sigma_\gamma^*)} d_{\sigma_\gamma, s_1}^{1/2} V_{\sigma_\gamma^*}^{s_1} \mathcal{M}_{n_1, n_2} \frac{\cos[\dots]}{\Delta}, \end{aligned} \quad (\text{B1})$$

where the last term on the third line reads $\frac{\cos[(\sigma_\Lambda - j_\gamma - \tilde{m}_2)\delta_1 - \tilde{m}_2\delta_2]}{p_{1\perp} p_{2\perp} \sin(\delta_1 + \delta_2)/2}$ and the positron spinor is expanded as $v_{s_1} = \sum_{\sigma_1^*} e^{-i\sigma_1^* \varphi_1} d_{\sigma_1^*, s_1}^{1/2} V_{\sigma_1^*}^{s_1}$, as in Eq. (7). After performing the summation and taking the Kronecker deltas in Eq. (A3) into account, we are left with the summation over n_1, n_2 , and

σ_1^* , accompanied by the vortex phase term $e^{-i(j_\gamma + \Delta n - s_1 + \sigma_1^*)\varphi_1}$. Therefore, Eq. (B1) represents a superposition of vortex modes with various Δn values, with each mode carrying TAM $j_1 = j_\gamma + \Delta n - s_2$.

-
- [1] L. Allen, M. W. Beijersbergen, and R. Spreeuw *et al.*, Orbital angular momentum of light and the transformation of Laguerre-Gaussian laser modes, *Phys. Rev. A* **45**, 8185 (1992).
 - [2] K. Y. Bliokh, I. P. Ivanov, and G. Guzzinati *et al.*, Theory and applications of free-electron vortex states, *Phys. Rep.* **690**, 1 (2017).
 - [3] S. Lloyd, M. Babiker, G. Thirunavukkarasu, and J. Yuan, Electron vortices: Beams with orbital angular momentum, *Rev. Mod. Phys.* **89**, 035004 (2017).
 - [4] B. A. Knyazev and V. Serbo, Beams of photons with nonzero projections of orbital angular momenta: new results, *Phys. Usp.* **61**, 449 (2018).
 - [5] I. P. Ivanov, N. Korchagin, A. Pimikov, and P. Zhang, Doing spin physics with unpolarized particles, *Phys. Rev. Lett.* **124**, 192001 (2020).
 - [6] D. Budker, M. Gorchtein, and A. Surzhykov *et al.*, Expanding nuclear physics horizons with the Gamma Factory, *Annalen Phys.* **534**, 2100284 (2021).
 - [7] I. P. Ivanov, Promises and challenges of high-energy vortex states collisions, *Prog. Part. Nucl. Phys.* **127**, 103987 (2022).
 - [8] Z.-W. Lu *et al.*, Manipulation of Giant Multipole Resonances via Vortex γ Photons, *Phys. Rev. Lett.* **131**, 202502 (2023).
 - [9] M. Benedikt, A. Blondel, P. Janot, M. Mangano, and F. Zimmermann, Future Circular Colliders succeeding the LHC, *Nature Phys.* **16**, 402 (2020).
 - [10] V. Shiltsev and F. Zimmermann, Modern and Future Colliders, *Rev. Mod. Phys.* **93**, 015006 (2021).
 - [11] D. P. Anderle *et al.*, Electron-ion collider in China, *Front. Phys. (Beijing)* **16**, 64701 (2021).
 - [12] C. A. Aidala, S. D. Bass, D. Hasch, and G. K. Mallot, The Spin Structure of the Nucleon, *Rev. Mod. Phys.* **85**, 655 (2013).
 - [13] E. Leader and C. Lorcé, The angular momentum controversy: What's it all about and does it matter?, *Phys. Rept.* **541**, 163 (2014).
 - [14] H. Larocque, I. Kaminer, V. Grillo, R. W. Boyd, and E. Karimi, Twisting neutrons may reveal their internal structure, *Nature Phys.* **14**, 1 (2018).
 - [15] G. M. Vanacore, G. Berruto, I. Madan, E. Pomarico, P. Biagioni, R. J. Lamb, D. McGrouther, O. Reinhardt, I. Kaminer, B. Barwick, H. Larocque, V. Grillo, E. Karimi, F. J. García de Abajo, and F. Carbone, Ultrafast generation and control of an electron vortex beam via chiral plasmonic near fields, *Nature Mater.* **18**, 573 (2019).
 - [16] J. Verbeeck, H. Tian, and P. Schattschneider, Production and application of electron vortex beams, *Nature* **467**, 301 (2010).
 - [17] A. Béché, R. Van Boxem, G. Van Tendeloo, and J. Verbeeck, Magnetic monopole field exposed by electrons, *Nature Phys.* **10**, 26 (2014).
 - [18] V. Grillo, G. C. Gazzadi, E. Mafakheri, S. Frabboni, E. Karimi, and R. W. Boyd, Holographic Generation of Highly Twisted Electron Beams, *Phys. Rev. Lett.* **114**, 034801 (2015).
 - [19] C. W. Clark, R. Barankov, M. G. Huber, M. Arif, D. G. Cory, and D. A. Pushin, Controlling neutron orbital angular momentum, *Nature* **525**, 504 (2015).
 - [20] A. Luski, Y. Segev, R. David, O. Bitton, H. Nadler, A. R. Barnea, A. Goriach, O. Cheshnovsky, I. Kaminer, and E. Narevicius, Vortex beams of atoms and molecules, *Science* **373**, 1105 (2021).
 - [21] D. Sarenac, J. Nsofini, I. Hincks, M. Arif, C. W. Clark, D. G. Cory, M. G. Huber, and D. A. Pushin, Methods for preparation and detection of neutron spin-orbit states, *New J. Phys.* **20**, 103012 (2018).
 - [22] D. Sarenac, C. Kapahi, W. Chen, C. W. Clark, D. G. Cory, M. G. Huber, I. Tamirniau, K. Zhernenkov, and D. A. Pushin, Generation and detection of spin-orbit coupled neutron beams, *Proc. Natl. Acad. Sci.* **116**, 20328 (2019).
 - [23] D. Sarenac, M. E. Henderson, H. Ekinici, C. W. Clark, D. G. Cory, L. Debeer-Schmitt, M. G. Huber, C. Kapahi, and D. A. Pushin, Experimental realization of neutron helical waves (2022), arXiv:2205.06263 [physics.app-ph].
 - [24] A. J. Silenko, P. Zhang, and L. Zou, Manipulating Twisted Electron Beams, *Phys. Rev. Lett.* **119**, 243903 (2017).
 - [25] A. J. Silenko, P. Zhang, and L. Zou, Relativistic quantum dynamics of twisted electron beams in arbitrary electric and magnetic fields, *Phys. Rev. Lett.* **121**, 043202 (2018).
 - [26] A. J. Silenko and O. V. Teryaev, Siberian snake-like behavior for an orbital polarization of a beam of twisted (vortex) electrons, *Phys. Part. Nucl. Lett.* **16**, 77 (2019).
 - [27] U. D. Jentschura and V. G. Serbo, Generation of high-energy photons with large orbital angular momentum by Compton backscattering, *Phys. Rev. Lett.* **106**, 013001 (2011).
 - [28] U. D. Jentschura and V. G. Serbo, Compton upconversion of twisted photons: backscattering of particles with non-planar wave functions, *Eur. Phys. J. C* **71**, 1 (2011).
 - [29] I. P. Ivanov, Creation of two vortex-entangled beams in a vortex-beam collision with a plane wave, *Phys. Rev. A* **85**, 033813 (2012).
 - [30] R. Van Boxem, B. Partoens, and J. Verbeeck, Inelastic electron-vortex-beam scattering, *Phys. Rev. A* **91**, 032703 (2015).
 - [31] D. V. Karlovets, S. S. Baturin, G. Geloni, G. K. Sitykh, and V. G. Serbo, Generation of vortex particles via generalized measurements, *Eur. Phys. J. C* **82**, 1008 (2022).
 - [32] D. V. Karlovets, S. S. Baturin, G. Geloni, G. K. Sitykh, and V. G. Serbo, Shifting physics of vortex particles to higher energies via quantum entanglement, *Eur. Phys. J. C* **83**, 372 (2023).
 - [33] S. Barnett, *Quantum Information* (Oxford University Press, 2009).
 - [34] M. A. Al Khafaji, C. M. Cisowski, H. Jimbrow, S. Croke, S. Pádua, and S. Franke-Arnold, Single-shot characterization of vector beams by generalized measurements, *Optics Express* **30**, 22396 (2022).

- [35] G. Breit and J. A. Wheeler, Collision of two light quanta, *Phys. Rev.* **46**, 1087 (1934).
- [36] H. Bethe and W. Heitler, On the Stopping of fast particles and on the creation of positive electrons, *Proc. Roy. Soc. Lond. A* **146**, 83 (1934).
- [37] J. W. Motz, H. A. Olsen, and H. W. Koch, Pair production by photons, *Rev. Mod. Phys.* **41**, 581 (1969).
- [38] Y.-S. Tsai, Pair Production and Bremsstrahlung of Charged Leptons, *Rev. Mod. Phys.* **46**, 815 (1974), [Erratum: *Rev. Mod. Phys.* **49**, 421–423 (1977)].
- [39] S. R. Klein, e^+e^- pair production from 10-GeV to 10-ZeV, *Radiat. Phys. Chem.* **75**, 696 (2006).
- [40] M. Aaboud *et al.* (ATLAS), Evidence for light-by-light scattering in heavy-ion collisions with the ATLAS detector at the LHC, *Nature Phys.* **13**, 852 (2017).
- [41] J. Adam *et al.* (STAR), Measurement of e^+e^- Momentum and Angular Distributions from Linearly Polarized Photon Collisions, *Phys. Rev. Lett.* **127**, 052302 (2021).
- [42] J. D. Brandenburg, J. Seger, Z. Xu, and W. Zha, Report on progress in physics: observation of the Breit–Wheeler process and vacuum birefringence in heavy-ion collisions, *Rept. Prog. Phys.* **86**, 083901 (2023).
- [43] Z. Bu, L. Ji, S. Lei, H. Hu, X. Zhang, and B. Shen, Twisted Breit-Wheeler electron-positron pair creation via vortex gamma photons, *Phys. Rev. Res.* **3**, 043159 (2021).
- [44] S. Lei, Z. Bu, W. Wang, B. Shen, and L. Ji, Generation of relativistic positrons carrying intrinsic orbital angular momentum, *Phys. Rev. D* **104**, 076025 (2021).
- [45] S. Lei, S. Liu, W. Wang, Z. Bu, B. Shen, and L. Ji, Transfer of spin to orbital angular momentum in the Bethe-Heitler process, *Phys. Rev. D* **108**, 036001 (2023).
- [46] S. Weber *et al.*, P3: An installation for high-energy density plasma physics and ultra-high intensity laser–matter interaction at ELI-Beamlines, *Matter Radiat. Extremes* **2**, 149 (2017).
- [47] E. Cartlidge, The light fantastic, *Science* **359**, 382 (2018).
- [48] C. N. Danson, C. Haefner, and J. Bromage *et al.*, Petawatt and exawatt class lasers worldwide, *High Power Laser Sci. Eng.* **7**, e54 (2019).
- [49] J. W. Yoon, C. Jeon, and J. Shin *et al.*, Achieving the laser intensity of 5.5×10^{22} W/cm² with a wavefront-corrected multi-PW laser, *Opt. Express* **27**, 20412 (2019).
- [50] J. W. Yoon, Y. G. Kim, I. W. Choi, J. H. Sung, H. W. Lee, S. K. Lee, and C. H. Nam, Realization of laser intensity over 10^{23} W/cm², *Optica* **8**, 630 (2021).
- [51] A. Di Piazza, C. Muller, K. Z. Hatsagortsyan, and C. H. Keitel, Extremely high-intensity laser interactions with fundamental quantum systems, *Rev. Mod. Phys.* **84**, 1177 (2012).
- [52] A. Gonoskov, T. G. Blackburn, M. Marklund, and S. S. Bulanov, Charged particle motion and radiation in strong electromagnetic fields, *Rev. Mod. Phys.* **94**, 045001 (2022).
- [53] A. Fedotov, A. Ilderton, F. Karbstein, B. King, D. Seipt, H. Taya, and G. Torgrimsson, Advances in QED with intense background fields, *Phys. Rept.* **1010**, 1 (2023).
- [54] S. S. Bulanov, C. Benedetti, D. Terzani, C. B. Schroeder, E. Esarey, T. Blackburn, and M. Marklund, A high-intensity laser-based positron source, (2023), arXiv:2311.10836 [physics.plasm-ph].
- [55] M. Vranic, O. Klimo, G. Korn, and S. Weber, Multi-GeV electron-positron beam generation from laser-electron scattering, *Sci. Rep.* **8**, 4702 (2018).
- [56] Y.-Y. Chen, P.-L. He, R. Shaisultanov, K. Z. Hatsagortsyan, and C. H. Keitel, Polarized positron beams via intense two-color laser pulses, *Phys. Rev. Lett.* **123**, 174801 (2019).
- [57] F. Wan, R. Shaisultanov, Y.-F. Li, K. Z. Hatsagortsyan, C. H. Keitel, and J.-X. Li, Ultrarelativistic polarized positron jets via collision of electron and ultraintense laser beams, *Phys. Lett. B* **800**, 135120 (2020).
- [58] Y.-F. Li, Y.-Y. Chen, W.-M. Wang, and H.-S. Hu, Production of Highly Polarized Positron Beams via Helicity Transfer from Polarized Electrons in a Strong Laser Field, *Phys. Rev. Lett.* **125**, 044802 (2020).
- [59] M. Büscher, A. Hützen, L. Ji, and A. Lehrach, Generation of polarized particle beams at relativistic laser intensities, *High Power Laser Sci. Eng.* **8**, e36 (2020).
- [60] H.-H. Song, W.-M. Wang, and Y.-T. Li, Dense Polarized Positrons from Laser-Irradiated Foil Targets in the QED Regime, *Phys. Rev. Lett.* **129**, 035001 (2022).
- [61] Y.-N. Dai, B.-F. Shen, J.-X. Li, R. Shaisultanov, K. Z. Hatsagortsyan, C. H. Keitel, and Y.-Y. Chen, Photon polarization effects in polarized electron–positron pair production in a strong laser field, *Matter Radiat. Extremes* **7**, 014401 (2022).
- [62] T. Sun, Q. Zhao, K. Xue, Z.-W. Lu, L.-L. Ji, F. Wan, Y. Wang, Y. I. Salamin, and J.-X. Li, Production of polarized particle beams via ultraintense laser pulses, *Rev. Mod. Plasma Phys.* **6**, 38 (2022).
- [63] K. Xue, T. Sun, K.-J. Wei, Z.-P. Li, Q. Zhao, F. Wan, C. Lv, Y.-T. Zhao, Z.-F. Xu, and J.-X. Li, Generation of High-Density High-Polarization Positrons via Single-Shot Strong Laser-Foil Interaction, *Phys. Rev. Lett.* **131**, 175101 (2023).
- [64] D. Y. Ivanov, G. L. Kotkin, and V. G. Serbo, Complete description of polarization effects in e^+e^- pair production by a photon in the field of a strong laser wave, *Eur. Phys. J. C* **40**, 27 (2005).
- [65] J. R. Danielson, D. H. E. Dubin, R. G. Greaves, and C. M. Surko, Plasma and trap-based techniques for science with positrons, *Rev. Mod. Phys.* **87**, 247 (2015).
- [66] M. J. A. Jansen, J. Z. Kamiński, K. Krajewska, and C. Müller, Strong-field Breit-Wheeler pair production in short laser pulses: Relevance of spin effects, *Phys. Rev. D* **94**, 013010 (2016).
- [67] D. Seipt and B. King, Spin- and polarization-dependent locally-constant-field-approximation rates for nonlinear Compton and Breit-Wheeler processes, *Phys. Rev. A* **102**, 052805 (2020).
- [68] G. Torgrimsson, Loops and polarization in strong-field QED, *New J. Phys.* **23**, 065001 (2021).
- [69] Y.-Y. Chen, K. Z. Hatsagortsyan, C. H. Keitel, and R. Shaisultanov, Electron spin- and photon polarization-resolved probabilities of strong-field QED processes, *Phys. Rev. D* **105**, 116013 (2022).
- [70] S. Tang, Fully polarized nonlinear Breit-Wheeler pair production in pulsed plane waves, *Phys. Rev. D* **105**, 056018 (2022).
- [71] K.-H. Zhuang, Y.-Y. Chen, Y.-F. Li, K. Z. Hatsagortsyan, and C. H. Keitel, Laser-driven lepton polarization in the quantum radiation-dominated reflection regime, *Phys. Rev. D* **108**, 033001 (2023).
- [72] Y.-Y. Chen, J.-X. Li, K. Z. Hatsagortsyan, and C. H. Keitel, γ -Ray Beams with Large Orbital Angular Momentum via Nonlinear Compton Scattering with Radiation Reaction, *Phys. Rev. Lett.* **121**, 074801 (2018).
- [73] X.-L. Zhu, T.-P. Yu, M. Chen, S.-M. Weng, and Z.-M. Sheng, Generation of GeV positron and γ -photon beams with controllable angular momentum by intense lasers, *New J. Phys.* **20**, 083013 (2018).
- [74] J. Zhao, Y.-T. Hu, Y. Lu, H. Zhang, L.-X. Hu, X.-L. Zhu, Z.-M. Sheng, I. C. E. Turcu, A. Pukhov, F.-Q. Shao, and T.-P. Yu, All-optical quasi-monoenergetic GeV positron bunch generation by twisted laser fields, *Commun. Phys.* **5**, 15 (2022).
- [75] C.-W. Zhang, D.-S. Zhang, and B.-S. Xie, Generation of γ -photons and pairs with transverse orbital angular mo-

- mentum via spatiotemporal optical vortex pulse, (2024), arXiv:2403.16414 [physics.optics].
- [76] V. I. Ritus, Quantum effects of the interaction of elementary particles with an intense electromagnetic field, *J. Russ. Laser Res.* **6**, 497 (1985).
 - [77] K. Y. Bliokh, M. R. Dennis, and F. Nori, Relativistic Electron Vortex Beams: Angular Momentum and Spin-Orbit Interaction, *Phys. Rev. Lett.* **107**, 174802 (2011).
 - [78] A. G. Hayrapetyan, O. Matula, A. Aiello, A. Surzhykov, and S. Fritzsche, Interaction of Relativistic Electron-Vortex Beams with Few-Cycle Laser Pulses, *Phys. Rev. Lett.* **112**, 134801 (2014).
 - [79] V. N. Baier, V. M. Katkov, and V. M. Strakhovenko, *Electromagnetic processes at high energies in oriented single crystals* (1998).
 - [80] T. N. Wistisen, Numerical approach to the semiclassical method of pair production for arbitrary spins and photon polarization, *Phys. Rev. D* **101**, 076017 (2020).
 - [81] D. Seipt, V. Kharin, and S. Rykovanov *et al.*, Analytical results for nonlinear Compton scattering in short intense laser pulses, *J. Plasma Phys.* **82**, 655820203 (2016).
 - [82] K. Y. Bliokh and F. Nori, Transverse and longitudinal angular momenta of light, *Phys. Rept.* **592**, 1 (2015).
 - [83] E. Leader, The photon angular momentum controversy: Resolution of a conflict between laser optics and particle physics, *Phys. Lett. B* **756**, 303 (2016).
 - [84] Y. Taira, T. Hayakawa, and M. Katoh, Gamma-ray vortices from nonlinear inverse Thomson scattering of circularly polarized light, *Sci. Rep.* **7**, 1 (2017).
 - [85] O. V. Bogdanov, P. Kazinski, and G. Y. Lazarenko, Semiclassical probability of radiation of twisted photons in the ultrarelativistic limit, *Phys. Rev. D* **99**, 116016 (2019).
 - [86] D. V. Karlovets, V. G. Serbo, and A. Surzhykov, Wave function of a photon produced in the resonant scattering of twisted light by relativistic ions, *Phys. Rev. A* **104**, 023101 (2021).
 - [87] M. Ababekri, R.-T. Guo, F. Wan, B. Qiao, Z. Li, C. Lv, B. Zhang, W. Zhou, Y. Gu, and J.-X. Li, Vortex γ photon generation via spin-to-orbital angular momentum transfer in nonlinear Compton scattering, *Phys. Rev. D* **109**, 016005 (2024).
 - [88] R.-T. Guo, M. Ababekri, Q. Zhao, Y. I. Salamin, L.-L. Ji, Z.-G. Bu, Z.-F. Xu, X.-F. Weng, and J.-X. Li, Generation of γ photons with extremely large orbital angular momenta, (2023), arXiv:2310.16306 [hep-ph].
 - [89] D. L. Burke *et al.*, Positron production in multi - photon light by light scattering, *Phys. Rev. Lett.* **79**, 1626 (1997).
 - [90] H. Hu, C. Muller, and C. H. Keitel, Complete QED theory of multiphoton trident pair production in strong laser fields, *Phys. Rev. Lett.* **105**, 080401 (2010).
 - [91] A. J. Macleod (LUXE), From theory to precision modelling of strong-field QED in the transition regime, *J. Phys. Conf. Ser.* **2249**, 012022 (2022).
 - [92] F. C. Salgado *et al.*, Single particle detection system for strong-field QED experiments, *New J. Phys.* **24**, 015002 (2022).
 - [93] H. Abramowicz *et al.*, Conceptual design report for the LUXE experiment, *Eur. Phys. J. ST* **230**, 2445 (2021).
 - [94] C. Schaerf, Polarized gamma-ray beams, *Phys. Today* **58**, 44 (2005).
 - [95] H. R. Weller, M. W. Ahmed, H. Gao, W. Tornow, Y. K. Wu, M. Gai, and R. Miskimen, Research opportunities at the upgraded hiys facility, *Prog. Part. Nucl. Phys.* **62**, 257 (2009).
 - [96] S. Tang, B. King, and H. Hu, Highly polarised gamma photons from electron-laser collisions, *Phys. Lett. B* **809**, 135701 (2020).
 - [97] D. Seipt, V. Y. Kharin, and S. G. Rykovanov, Optimizing Laser Pulses for Narrow-Band Inverse Compton Sources in the High-Intensity Regime, *Phys. Rev. Lett.* **122**, 204802 (2019).
 - [98] V. Petrillo, I. Drebot, M. Ruijter, S. Samsam, A. Bacci, C. Curatolo, M. Oromolla, M. R. Conti, A. R. Rossi, and L. Serafini, State of the art of high-flux compton/thomson x-rays sources, *Appl. Sci.* **13**, 10.3390/app13020752 (2023).
 - [99] I. P. Ivanov, Colliding particles carrying non-zero orbital angular momentum, *Phys. Rev. D* **83**, 093001 (2011).
 - [100] V. B. Berestetskii, E. M. Lifshitz, and L. P. Pitaevskii, *QUANTUM ELECTRODYNAMICS* (Pergamon Press, 1982).